# On-Chip Photonic Crystal Surface-Emitting Membrane Lasers (Invited)

Weidong Zhou, *Senior Member, IEEE*, Shih-Chia Liu, Xiaochen Ge, Deyin Zhao, Hongjun Yang, Carl Reuterskiöld-Hedlund, and Mattias Hammar

***Abstract*—Photonic crystal lasers can be realized either based on photonic bandgap defect mode or defect-free bandedge mode, while the bandgap is not essential for the latter. We review here defect-free bandedge mode based photonic crystal surface-emitting lasers (PCSELs) for on-chip integration. We first discuss ultra-thin membrane reflector vertical-cavity surface-emitting lasers (MR-VCSELs), where single layer photonic crystal slabs can be designed as a broadband membrane reflector. Later, we discuss another type of defect-free PCSELs where the lasing cavity is formed based on evanescent coupling of gain medium with the photonic crystal bandedge mode near bandedge. Cavity designs were carried out for the optimal modal overlap and high confinement factors. Lateral cavity size scaling was also investigated both theoretically and experimentally in PCSELs. Buried tunnel junction (BTJ) based InGaAsP quantum well (QW) heterostructures were also designed and incorporated into electrically injected PCSELs. Finally discussions are given towards energy efficient lasers.**

***Index Terms*— Heterogeneous integration, photonic crystals, silicon photonics, surface-emitting lasers.**

## I. Introduction

Silicon-based light sources have witnessed significant advances over the last decade, with one of the most promising approaches being heterogeneous integration of various Si-based laser cavities on SOI substrates [1-9]. Photonic crystals have been known to be an excellent candidate for ultra-compact energy efficient lasers via spontaneous emission control and dispersion engineering. Based on defect mode cavities and defect-free bandage effects, Lasers have been reported for low power single photon sources as well as high power single mode broad area laser sources, mostly on III-V substrates [10-16]. Additionally, based on Fano resonance or guided resonance principles, broadband single layer membrane reflectors (MR) can also be designed based on photonic crystal cavities in constructing VCSELs [17-19].

Here, we report design and analysis of photonic crystal surface-emitting membrane lasers for silicon photonics, based on printed IIII-V QW heterostructures heterogeneously integrated on Si-based photonic crystal cavities. Based on the evanescent mode coupling, membrane lasers can be realized by vertical-coupling of III-V QW membranes on defect-mode and bandage photonic crystal cavities on Si. The effect of coupling strength and mode overlap on confinement factor and lasing threshold will be evaluated and optimized. On the other hand, based on photonic crystal membrane reflectors, MR-VCSEL cavities can be design with the proper selection of low index buffer layers between the photonic crystal membrane reflectors and III-V QW structures. Both photonic crystal guided resonance mode and Fabry-Perot lasing cavity mode need to be properly controlled. Earlier, printed large-area single-mode MR-VCSELs and PCSELs on SOI substrates were reported [20]. Here, optically and electrically pumped laser characteristics will be discussed, with the results compared with the gain threshold conditions for lasing model property analysis. Cavity scaling and electrical injection will also be discussed for practical and energy efficient source on-chip for integrated photonics.

## II. Overview of Photonic Crystal Lasers

Photonic crystals (PC) were proposed initially for spontaneous emission control and low threshold lasers [21]. Since then, many types of lasers have been reported. Based on the functions of photonic crystal structures, these lasers can largely be characterized as one of the following three types (Fig. 1):

(I) *Photonic bandgap defect mode lasers (PBDL):* By incorporating defect states inside otherwise perfect photonic bandgap (PBG), spontaneous emission can be enhanced only at localized defect states, while suppressed at all other energy levels within the PBG region. Based on this principle, light sources were demonstrated with high spontaneous emission factors. Active regions of the light emitters were embedded inside these PBG photonic crystal structures. [21, 22] By engineering the optical quality factor Q and optical cavity modal volume V, spontaneous emission control can be realized, which can result in ultra-low threshold lasers [23-29]. Another architecture reported recently [30] is the coupling of un-patterned ultrathin monolayer tungsten diselenide monolayer gain medium

Manuscript received August 2, 2018.

This work was supported in part by the US Army Research Office under grants W911NF-09-1-0505 and W911NF-15-1-0431 (PM: Dr. Michael Gerhold), and by the U.S. Air Force of Scientific Research under Grant FA9550-11-C-0026 (PM: Dr. Gernot Pomrenke). M.H. acknowledges the support from the Swedish Research Council (VR 201603388).

W. D. Zhou, S. Liu, X. Ge, D. Zhao, and H. Yang are with Department of Electrical Engineering, the University of Texas at Arlington, Arlington, TX 76019, USA (e-mail: wzhou@uta.edu).

C. Reuterskiöld-Hedlund and M. Hammar are with Department of Electronics, Royal Institute of Technology, Electrum 229, 164 40 Kista, Sweden.

This article has been accepted for publication in a future issue of this journal, but has not been fully edited. Content may change prior to final publication. Citation information: DOI 10.1109/JSTQE.2019.2902904, IEEE Journal of Selected Topics in Quantum Electronics



with the defect mode photonic crystal cavity. This configuration can lead to higher efficiency lasers as no-patterned or etching is done on the gain medium. Challenges may lie on the trade-offs in the desired high *Q* cavity inside the photonic bandgap and the high coupling efficiency between the high index gain medium and photonic crystal cavities.

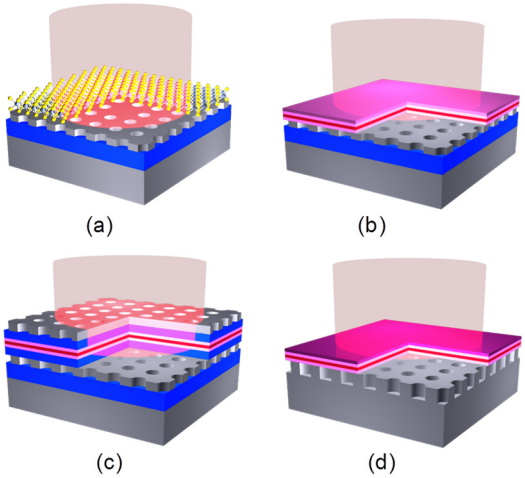


Fig. 1. Si-based photonic crystal cavities for membrane lasers: (a) Photonic crystal defect-mode lasers on SOI; (b) Photonic crystal bandedge lasers on SOI; (c) Photonic crystal MR-VCSELs on SOI; and (d) Photonic crystal bandedge lasers on bulk Si.

*(II)Photonic bandedge lasers (PBEL): Defect-free p*hotonic crystal structure can also be used to realized photonic bandedge lasers, where the lasing cavity can be formed based on the bandage effect. Lasing is based on the coherent feedback associated with these bandedge modes, based on first and second Bragg scattering principles. Different from PBDL, these cavity modes are typically located above lightline, thus these lasers are intrinsically leaky and surface-emitting, which can result in excellent beam qualities. Over the years, high performance PBEL lasers have been reported with excellent performance, mostly on native substrates. Large area PBELs were demonstrated with single longitudinal and transverse mode, high optical power, and optical beam and pattern control [16, 31-35].

*(III) Membrane reflector VCSEL (MR-VCSELs):* Photonic crystals can also serve as single layer broadband reflectors, based on guided or Fano resonance principles. These ultra-compact high performance single layer 1D or 2D PCS membrane reflectors (MRs) have been proposed to create ultra-compact DBR-free MR-VCSELs [20, 36]. Most importantly, such MR-VCSELs cam be formed on any substrates at any wavelengths. The scaling properties is especially attractive in realizing longer wavelength VCSELs, where conventional DBRs is either too bulky or impossible to achieve.

Among three configurations discussed above, PBG properties is required for PBDL laser, where the localized defect mode is designed towards lasing. However, PBG is not essential for two other types of lasers (PBEL and MR-VCSEL), as both utilize propagating modes in defect-free PCS structures. Additionally, the defect mode laser in PBDLs operates with the modes below lightline. On the other hand, defect-free PBEL can utilize the mode both below and above the light lines [37]. It is also worth mentioning that since photonic bandgap is not required in PBEL, the requirement on high index contrast can be relaxed. Lasing cavities can be built directly on patterned bulk semiconductor InP or Si substrates (Fig. 1(d)).

Additionally, Photonic crystal structures are also incorporated in the semiconductor lasers, for mode control and beam steering [28, 29, 38, 39]. It may also lead to novel emitters based on gain/loss engineering and parity-time symmetry control.

## III. Photonic Crystal MR-VCSEL Cavity Design

### *A. Photonic crystal Membrane Reflectors (MR)*

Reflection spectral bandwidth is one of the key design targets for broadband reflectors. The broadband reflection principles are quite different between conventional DBR-based reflectors and the photonic crystal based MRs. Theoretical analysis was reported on the broadband reflector mechanisms from 1D PC/grating structures. It was contributed to the coupling of leaky modes and their excitation conditions [40], Or destructive coupling at different interfaces. [41] For 2D PCS based MRs, the designs are largely based on the trial-and-error approaches based on complete 3D computations, such as rigorous coupled-wave analysis (RCWA) and finite-difference time domain (FDTD) techniques. Based on the different designs for high *Q* filters and broadband MRs, researchers found that the *Q* factor (spectral linewidth) can be controlled by varying the radius, with very small *r*/*a* values (~0.1) favoring high *Q* filter designs and large *r*/*a* values (0.3-0.49) favoring broadband reflector designs. Other design parameters include the lattice structure and the air hole shape, the buffer layer selection below and above the functional layer, effective indices, and so on.[19]

High reflectivity for surface-normal direction originates from the modal coupling between vertical radiation modes and discrete in-plane guide modes. As shown in Fig. 2(a), multiple Fano resonance modes can be identified from the simulated transmission spectrum (log plot). It is worth noting that we plot the transmission in log scale in order to show multiple resonances within the broadband reflection window. At Fano resonances (e.g. 1500 nm shown in Fig. 2(b)), there is a coupling between in-plane guided mode (inside Si-MR) and vertical cavity mode which results in a destructive interference in the direction of transmission.

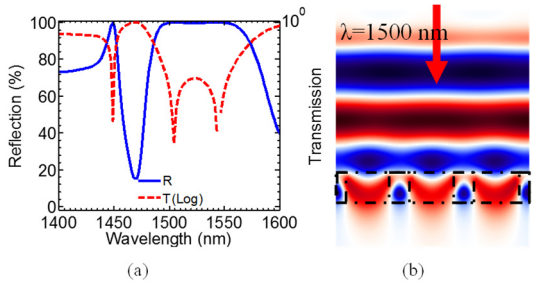


Fig. 2. Fano resonance membrane reflector (MR) design and modal coupling: (a) Simulated reflection (blue) and transmission (red) spectra for the Fano MR; and (b) Simulated field distribution profiles for the design shown in (a) at one Fano resonance location (λ = 1500 nm). Notice the dash box/lines indicating the air hole photonic crystal layer.

This article has been accepted for publication in a future issue of this journal, but has not been fully edited. Content may change prior to final publication. Citation information: DOI 10.1109/JSTQE.2019.2902904, IEEE Journal of Selected Topics in Quantum Electronics



Qiang *et al.* [42] demonstrated the design of control of reflection bands based on the control of vertical confinement, where the refractive indexes for the buffer layers below and above the MR layer can be carefully tuned. Yang *et al.* [43] reported experimental demonstrations, where a controlled index tuning range over 50 nm for both blue and red shifts were realized, by controlled etching in the buried oxide layer below, and the controlled oxide deposition above.

### *B. Energy and phase penetration properties*

While the absolute reflectivity is important in dielectric mirror design, the energy penetration depth $L_e$ and the phase discontinuity $\Phi_r$ are two additional important parameters to be considered. The reflection is not an instantaneous process. It includes energy storage in the mirrors, and a reflection time delay ($\tau$). The reflection time delay leads to an increase in the laser cavity round-trip time or the photon lifetime. The energy storage in mirrors results in a decrease of the modal volume and the confinement factor [20, 21]. The reflection delay is directly related to the slope of the reflection phase shift $\Phi_r$. The relation can be expressed as $\tau = \partial\Phi_r / \partial\omega$. The phase penetration depth, $L_p$, is defined as the half-distance that light propagates in the incident medium during this delay time,

$$L_p = \frac{1}{2} v_g \tau = \frac{v_g}{2} \frac{\partial \Phi_r}{\partial \omega} \tag{1}$$

where $v_g$ is the group velocity of the incident wave.

Similarly, the energy penetration depth parameter, $L_e$, is used to quantify the energy storage of the mirror. It is the length that the field intensity decays to *1*/e of its maximum from the edge of the cavity into the mirrors. For conventional dielectric distributed Bragg reflectors (DBRs), $L_e$ can be obtained with [44]:

$$L_e = \frac{m_{eff}}{2} \left( \frac{\lambda}{4n_1} + \frac{\lambda}{4n_2} \right) \tag{2}$$

where $m_{\text{eff}} = \tanh(2mr)/(2r)$ is the effective period number seen by the incident light. $r=(n_1-n_2)/(n_1+n_2)$ and $m$ are the actual period number in DBRs. $n_1$ and $n_2$ are the refractive index of the two materials in DBR.

However, the above equation is not suitable for calculating the $L_e$ of the photonic crystal PC mirrors we discussed here. The guided modes are excited inside the mirrors. But $L_e$ can be estimated from the mirror transmission or reflection based on the following equation,

$$T = 1 - R = \exp\left(-\frac{h}{L_e}\right) \tag{3}$$

where $T$ is the transmission and $h$ is the mirror thickness [45, 46].

According to the above definitions, Zhao *et al.* [46] numerically investigated the phase and energy penetration depths for different types of dielectric mirrors. The results are shown in Fig. 3 for a set of 1550 nm reflector designs. Different from the DBR reflectors, single layer PC MRs have larger phase delays with larger spectral dependent properties. Yet, smaller energy penetration properties was evident, due to strong localized mode and strong optical confinement associated with larger index contrasts. These properties can all be engineered via dispersion engineering. Following similar procedures, reflectors with different reflection requirements can be designed.

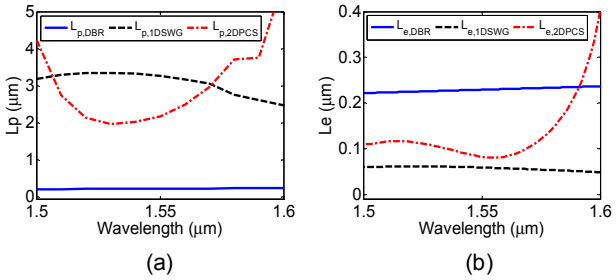


Fig. 3. (a) Calculated phase penetration depths for three types of reflectors; and (b) The energy penetration depths for three types of reflectors. [46]

### *C. Membrane reflector vertical-cavity surface-emitting lasers*

Shown in Fig. 4(a) is the schematic of a MR-VCSEL on Si substrate, where a gain layer (e.g. QWs) is sandwiched in between two single layer Si MRs. Low index buffer layers are incorporated below and above the high index Si MR layer, desired for the proper high reflection MR design.

The cavity resonance mode were extracted from the simulated reflection spectrum (blue line shown in Fig. 4(b)), where the dip appears around 1478 nm, which corresponds to the cavity resonance mode. This mode was also validated with the phase discontinuity shown in the simulated total phase change in the cavity (red dash line shown in Fig. 4(b)).

The cavity mode quality factor Q can then be simulated with FDTD technique with a short temporal Gaussian pulse to excite the cavity mode at 1478 nm. For this specific design, Q of 4300 was obtained according to $Q = \text{Re}(\omega) / 2 \cdot \text{Im}(\omega)$ [47]. The filed distribution profile shown in Fig. 4(c) was obtained with a longer temporal Gaussian pulse excitation. Also shown in Fig. 4(c) is the cavity index profile.

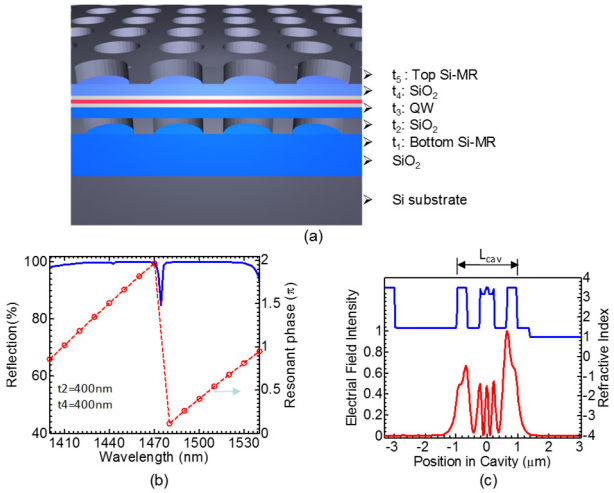


Fig. 4. Characteristics of designed MR-VCSEL cavity: (a) Schematic of MR-VCSEL; (b) Calculated cavity resonance mode based on cavity reflection and phase resonant condition; and (c) Field distribution of cavity mode.

Another design concern that needs to be taken care of is the separation the lasing cavity modes from the QW layer as mentioned in a Ref. [48]. Despite the relatively large field concentration in Si-MR layers, the lasing mode field confinement factor is 5.6% for MR-VCSELs, which is

This article has been accepted for publication in a future issue of this journal, but has not been fully edited. Content may change prior to final publication. Citation information: DOI 10.1109/JSTQE.2019.2902904, IEEE Journal of Selected Topics in Quantum Electronics



comparable to DBR-based VCSELs. This critical feature enables low threshold lasing in the MR-VCSEL cavities.

## IV. Photonic Crystal Bandedge Surface-Emitting Laser Cavity Design

The principle of the lasing modes in the photonic crystal surface emitting laser (PCSEL) cavities is based on the band edge modes of two-dimensional (2D) PC close to the second order Γ point [49-51], where the group velocities of these modes are close to zero. In such 2D PC cavities, the periodic patterned structure is designed close to the unpatented active region to provide strong in-plane distributed feedback (DFB) and the standing wave is formed in multiple directions due to the 2D DFB effect [49]. Simultaneously, the in-plane propagating waves are diffracted toward the vertical direction by the PC structure itself due to the first-order Bragg diffraction. It is because of this multidirectional Bragg diffraction in these 2D PC structures, the cavity mode can lase over a large 2D area and gives a high power output [16, 34].

Shown in Fig. 5(a) is a schematic of the PCSEL on Si SOI substrate, where an InGaAsP MQW heterostructure is stacked on a Si-PC cavity. The InGaAsP MQW layer is designed to have a center emission wavelength around 1550 nm, which consists of eight pairs of strain-compensated $In_{0.76}Ga_{0.24}As_{0.83}P_{0.17}/In_{0.485}Ga_{0.515}As_{0.83}P_{0.17}$ [52]. Here we consider two dimension square lattices Si-PC structure [53-59]. In addition to carefully design the cavity mode to match with the QW emission mode, the separation between the InGaAsP MQW layer and Si-PC slab is reduced to enhance the confinement factors and the in-plane coupling efficiency [60, 61].

### A. Bandedge mode design

The approximate effective refractive index $n_{eff}$ of the whole cavity is around 3.2. For the design of the PCSEL here with center wavelength around 1,550 nm, the lattice constant $a$ of the cavity is calculated to be 480 nm according to second Bragg diffraction condition $a = \lambda / n_{eff}$. To obtain high Q mode for low lasing threshold, the air hole radius is designed to be 72 nm ($r = 0.15a$) [52]. Si-PC slab e thickness is 190 nm [62].

Shown in Fig. 5(b) is a zoom-in band structure for Si-PC PCSEL cavity, where different modes near bandedge (k = 0, Γ point). It is obtained from the Fano resonances peaks or dips in the simulated reflection or transmission spectra according to the relation between the in-plane wave vector $k_{//}$ and the incident angle $\theta$, $k_{//} = 2\pi / \lambda \cdot \sin\theta$ [63], where λ is the wavelength and $\theta$ is the incident angle off the surface normal direction. By changing the incident angle from the surface normal direction (z-axis) to in-plane along the x-axis, the photonic bands in the Γ - X direction can be obtained. The Γ point corresponds to the surface-normal incidence $\theta = 0°$. Here we mainly focus on a small value range of incident angle $\theta$ from 0° to 2°, which corresponds to the $k_{//}$ range from 0 to ~0.01 ($2\pi/a$) in the vicinity of the band edge. The spectral simulation is done by the Fourier Modal Method with Stanford Stratified Structure Solver ($S^4$) software package. [64] In Fig. 5(b), the four bands in the normalized wavelength range (1,520 nm, 1,550 nm) are displayed with blue-solid lines for the transverse electric (TE, or *s*) polarization, and red-dashed lines for the transverse magnetic (TM, or *p*) polarization.

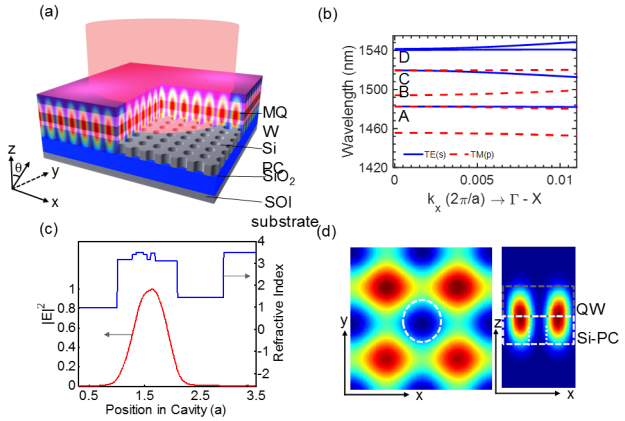


Fig. 5 (a) Schematic of PC bandedge membrane laser on SOI. (b) Photonic band diagram along Γ - X direction of Si-PC bandedge membrane laser cavity structure, with the transferred InGaAsP QW mesas on top. (c) Field distribution of cavity mode, and (d) Simulated field distributions.

Shown in Fig. 5(c) are the refractive index profile for the cavity, along with the calculated field profile for mode D shown in Fig. 5(b), with center wavelength of 1,540 nm. The confinement factor can be calculated as follows:

$$\Gamma_{QW} = \frac{\int_{QW} \varepsilon |E|^2 \bullet dv}{\int_{cav} \varepsilon |E|^2 \bullet dv} \tag{4}$$

The radiation loss for the cavity can be related to the cavity quality factor Q, with the following equation:

$$\alpha = \frac{2\pi}{Q \bullet a} \tag{5}$$

Where the quality factor Q can be derived from the Fano fitting of the resonances obtained in the reflection spectra [65]. Therefore, the gain threshold can be derived as follows:

$$g_{th} = \frac{\alpha}{\Gamma_{QW}} \tag{6}$$

The E-field along the center of cavity (left) and the cross-section views of the E-field intensity of modes (right) are shown in Fig. 5(d). One can see the field is strongly confined inside the cavity. Based on the above fundamental equations, the confinement factor, quality factor, and radiation loss of mode D (λ = 1,540 nm) is calculated to be 16.83%, $1.9 \times 10^5$ and 0.68 $cm^{-1}$, respectively. Single mode lasing can be predicted to occur at mode D which has the lowest gain threshold of 4.04 $cm^{-1}$.

### B. Lateral cavity scaling

For on-chip integration and for high performance lasers on-chip, it is highly desirable to have lasers with compact cavity volumes. In addition to shrinking the vertical cavity sizes, it is also important to reduce the lateral cavity size. However, one of the issues associated with the PCSEL device is the reduction in the optical confinement with the reduced lateral cavity size, which can result in increased lasing threshold and reduced lasing efficiency [66].

This article has been accepted for publication in a future issue of this journal, but has not been fully edited. Content may change prior to final publication. Citation information: DOI 10.1109/JSTQE.2019.2902904, IEEE Journal of Selected Topics in Quantum Electronics



To investigate the lateral confinement effect, we considered two control parameters. [67] We first consider gain confinement with the control of the optical pump beam spot size (Fig. 6(c)). We also consider index confinement with the etching of the mesa with different lateral dimensions and etch depths (Fig. 6(d)). Theoretical investigations were first carried out to estimate the cavity $Q$ factor and the associated gain thresholds for different lateral and vertical dimensions and then the corresponding threshold gains were estimated [68, 69].

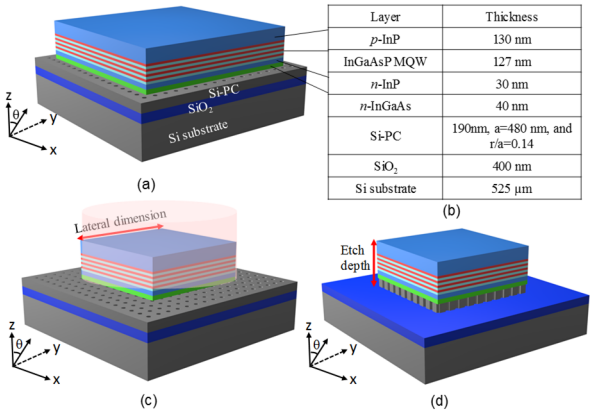


Fig. 6. (a) Schematic of PCSEL with 600 × 600 μm$^2$ size. (b) Cavity layer definitions. (c) Schematic of PCSEL with variation in lateral dimension (L). (d) Schematic of PCSEL with variation in vertical etch depth.

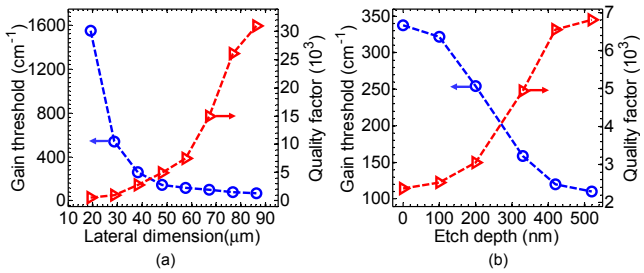


Fig. 7. (a) The simulated gain thresholds and Q factors for different device lateral dimensions; and (b) The simulated gain thresholds and Q factors for a device with lateral dimension of 48 μm (L = 100 $a$) at different etching depths. [67]

The calculated threshold gains and $Q$ factors are shown in Fig. 7(a). It can be seen that with decreasing device size from 80 μm to 20 μm, the $Q$ factor drops rapidly while the threshold gain increases. This indicates that the influence of in-plane loss has to be taken into account for finite device sizes.

Lateral cavity loss can be reduced by different lateral confinement schemes. With the control of the mesa etching depth, the lateral index contrast can be altered, which can result in different cavity losses. Shown in Fig. 7(b) are the measured quality factor and gain threshold for a PCSEL on Si with a lateral cavity dimension of 48 μm ($L$ = 100 $a$). By increasing the etch depth from 0 to 500 nm, which corresponds to the complete removal of the InGaAsP QW heterostructure and Si PC cavity (Fig. 6(d)), the cavity $Q$ factor increases from 2,300 to 6,800. We attribute this to the increased lateral confinement due to the increased lateral index contrast.

## V. Printed Membrane Laser Cavities

The integration of InGaAsP QW heterostructure with the Si photonic crystal structure was carried out with a printing process. For Si-MR/InGaAsP-QW/Si-MR MR-VCSEL cavity, two step printing processes are involved [20]. For the desired vertical index contrast, low index $SiO_2$ buffer layers are prepared between Si-MR and InGaAsP QW layers. It is noted such a requirement on the low index buffer can limit device performance due to poor thermal conductivity of the presence of low index $SiO_2$ buffer layers.

Different from the MR-VCSEL [20], PCSEL structure only requires a one-step printing process. Also, high index QW layer can be placed directly on the high index Si PC layer, without the low index buffer, In fact, it is critical to minimize the separation between QW layer and Si-PC cavity layer in order to obtain a high confinement factor which is critical to low threshold lasing.

Si PC cavity was first prepared based on standard electron beam lithography (EBL) and reactive ion etching (RIE) processes. Shown in Fig. 8(a) is a scanning electron microscopic (SEM) top view image of Si-PC on SOI substrate. The lattice constant $a$ and air hole radius $r$ of the fabricated PC are 480 nm and 72 nm, respectively.

MOCVD grown InGaAsP MQW structure [52] was then processed and transferred onto the patterned Si PC cavity directly, as shown in Fig. 8(b) and (c). Shown in Fig. 8(d) is a micrograph image of PC bandedge membrane lasers on SOI substrate. It is worth noting that this process could be applied at room temperature and is capable of a 5-μm alignment accuracy. Further improvement in alignment technical can result in sub-micron alignment accuracy.

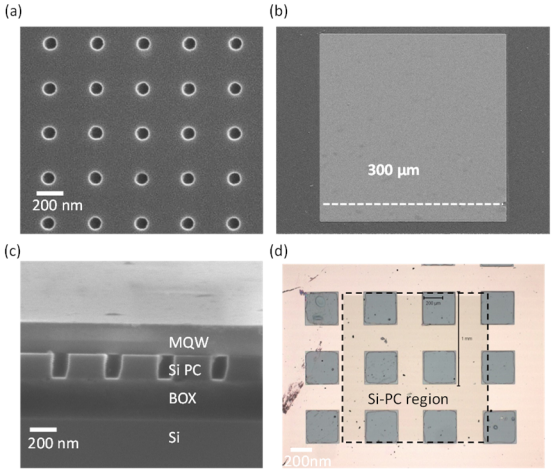


Fig. 8 (a) Zoomed-in SEM top view of the defect free Si-PC cavity. (b) An SEM image of InGaAsP MQW mesa transferred onto a Si-PC. (c) Cross-sectional view of the cavity, and (d) Micrograph image of the transferred mesa array on a Si-PC.

## VI. MR-VCSEL Characterization

Optically pumped devices are mounted inside a cryostat and characterized with a monochromator-based micro-photoluminescence (μ-PL) set up using quasi-continuous wave (c.w.) 532 nm laser pumping (with 50% duty cycle).

The measured output and the spectral linewidth is shown in Fig. 9(a) for different pump powers. A set of measured spectral outputs are shown in Fig. 9(b), corresponding to different pump powers (I, ii, iii, and iv) shown in Fig. 9(a). We see a linewidth change from 30 nm below threshold to 0.6-0.8

This article has been accepted for publication in a future issue of this journal, but has not been fully edited. Content may change prior to final publication. Citation information: DOI 10.1109/JSTQE.2019.2902904, IEEE Journal of Selected Topics in Quantum Electronics



nm above threshold. The threshold pump power is ~ 8mW, corresponding to a threshold density of 0.32kW/cm$^2$.

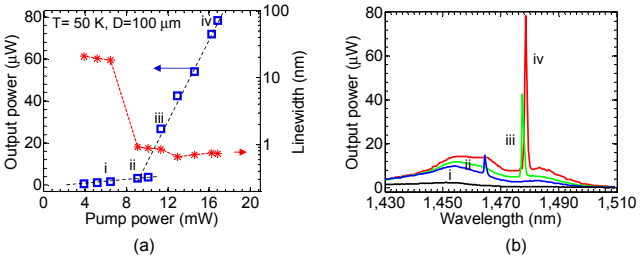


Fig. 9. (a), The L-L plot (light output for different pump powers) and the corresponding spectral linewidths at T = 50K; (b) The measured spectral outputs for pump powers below, at, and above thresholds. [18]

This MR-VCSEL was also characterized at different temperatures. Shown in Fig. 10(a) are the normalized lasing spectra at temperatures from $T$ = 15 K to T = 120 K. Notice the lasing peak red shifts as $T$ increases and multimode lasing for most $T$ cases at a rate ($d\lambda_c/dT$) close to the simulated 0.088 nm/K. There is a mode hopping occurred below and above the operation temperature of 80 K. As $T$ rises higher than 125K, there was no lasing any more, which is mainly limited by the MR reflector bandwidth. The laser characteristic temperature (T0) was derived to be 125 K, based on the measured temperature dependent threshold, as shown in Fig. 10 (b).

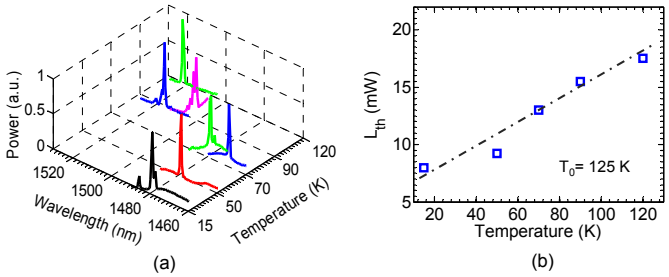


Fig. 10. (a) Measured lasing spectral at different temperatures under 532 nm laser pumping; (b) Lasing threshold as a function of temperature. [18]

TABLE 1 MR-VCSEL LASING THRESHOLD ESTIMATES

| Cavity types | MR-VCSEL on Si | DBR-VCSEL on InP |
|---|---|---|
| Top Reflector | Si NM MR | 5 pairs GaAs/Al $_x$O $_y$ DBR |
| Bottom Reflector | Si NM MR | InGaAsP/InP DBR |
| Wavelength $\lambda_{res}$ | 1.513 μm | 1.54 μm |
| Reflection $R_t$ | 98.2% (99.6%) | 99.6% |
| Reflection $R_b$ | 98.9% (99.6%) | 99.6% |
| Confinement Γ | 5.6% | 4.5% |
| Cavity length $L_{cav}$ | 1.21 μm | ~1.0 μm |
| Effective cavity $L_{eff}$ | 3.783 μm | ~13.1 μm |
| Cavity loss $\alpha_i+\alpha_{Si}$ | 40 cm$^{-1}$ | 43.1 cm$^{-1}$ |
| Gain threshold $g_{th}$ | 1283 cm$^{-1}$ (843 cm$^{-1}$) | 1224 cm$^{-1}$ |

Finally, lasing gain threshold can then be estimated, based on the cavity gain and loss characteristics reported earlier from similar QW structures [70]. The results are summarized in Table 1. Based on our design, MR-VCSEL can lase with a gain threshold of 840-1300 cm$^{-1}$, depending on the MR reflectivity.

For comparison, also shown in Table 1 are the typical parameters for long wavelength VCSELs based on conventional InGaAsP/InP DBRs. As can be seen, the MR-VCSEL has a very similar lasing gain threshold with conventional InGaAsP/InP DBR based VCSEL, even though MR-VCSELs have smaller cavities with much shorter effective cavity lengths (2.4 μm vs 5-20 μm) [71, 72]. Further optimization in the cavity design can lead to high performance MR-VCSELs with very low threshold and high efficiency.

## VII. PCSEL CHARACTERIZATION

Similarly, optically pumped PCSEL devices characterized with a 532 nm green laser with the excitation spot size around 110 μm. The measured outputs and spectral linewidths are shown in Fig. 11(a) for different pump power densities. A threshold power density of 0.25 kW/cm$^2$ was obtained. The measured spectral linewidth was reduced from ~14 nm (below threshold) to 0.54 nm (above threshold). Shown in Fig. 11(b) is a typical lasing spectrum above threshold, with laser wavelength of 1,542 nm. This corresponds to the predicted value of mode D shown in Fig. 5(b). The lower threshold pump power density is a result of the high $Q$ of mode D.

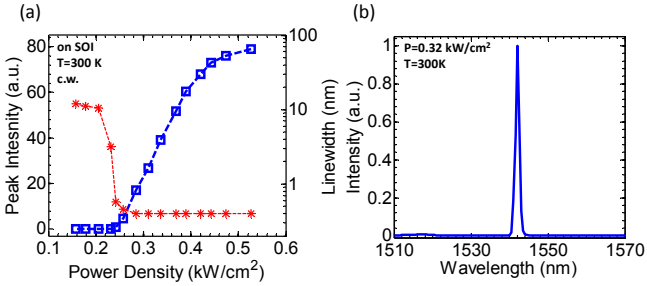


Fig. 11 (a) Lasing power and linewidth versus input power density at room temperature. (b) Emission spectrum of the laser above threshold.

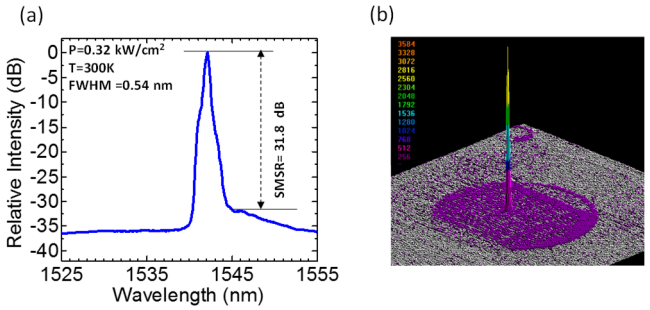


Fig. 12 (a) Lasing spectral output plotted in semi-log scale above the pumping threshold. (b) 3D far field laser profile.

Single mode operation was obtained for this large area (defined by the pump spot size of 110 μm) PCSEL on Si. As shown in Fig. 12(a), the full width at half maximum (FWHM) of the spectrum, and side mode suppression ratio (SMSR) are 0.54 nm and 31.8 dB, respectively. Fig. 12(b) is a measured far-field lasing profile with single mode output at the focusing plane of the collimator.

This article has been accepted for publication in a future issue of this journal, but has not been fully edited. Content may change prior to final publication. Citation information: DOI 10.1109/JSTQE.2019.2902904, IEEE Journal of Selected Topics in Quantum Electronics



## VIII. PCSEL ON BULK SILICON SUBSTRATE

The use of the $SiO_2$ in the laser structure may limit its thermal performance due to the relatively low thermal conductivity associated with the oxide layer. While oxide is not part of the lasing cavity in PCSELs, the use of SOI substrate can also present some issues related to thermal dissipation due to the thermal barriers between the top PCSEL cavity and the bottom Si substrates. So it is highly desirable to explore lasers built directly on bulk Si substrates. As mentioned earlier, index contrast is much more relaxed in PCSELs as only the dispersion engineering is used here. PBG is not needed. The design parameters were carefully chosen for the bottom Si-PC on bulk Si substrate.

A schematic of a successful design of this structure is shown in Fig. 13(a). The SEM cross-sectional view of PCSEL on bulk Si substrate is shown in Fig. 13(b). The lattice constant ($a$), air hole radius ($r$), and etched depth of the fabricated PC are 540 nm, 243 nm, and 400 nm, respectively. The approximate refractive index $n_{eff}$ of the InGaAsP MQW active layer and Si-PC was around 3.2 and 2.2 based on the average dielectric constant in the design. Here the relatively lower effective index of Si-PC layer also serves as the low index cladding layer between lasing cavity the bottom bulk Si substrate.

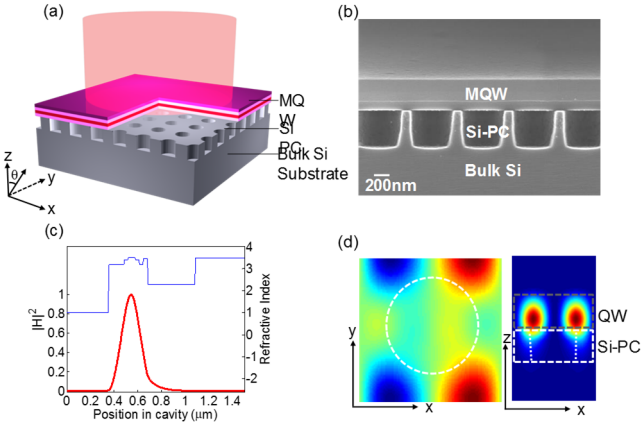


Fig. 13 (a) Schematic of PC bandedge membrane laser on bulk Si substrate. (b) Cross-sectional view of the Si-PC bandedge membrane laser cavity structure on bulk Si substrate, with the transferred InGaAsP QW mesas on top. (c) Field distribution of the cavity mode, and (d) Simulated in-plane and cross-sectional field distributions.

Shown in Fig. 13(c) is the field profile of the lasing mode, where the integrated H-field intensity of the whole cavity along the z-axis direction is plotted. Also shown in Fig. 13(c) is the cavity index profile. The cross-section views of H-field intensity of lasing mode are shown in Fig. 13(d). The field was strongly confined inside the thin cavity. To reduce the vertical radiation loss, the Si-PC slab was chosen to be 400 nm. This results in a Q value of 3,000 [12].

Shown in Fig. 14(a) are the measured light output and linewidth as a function of the pump power. The laser threshold pump power density of 0.4 kW/cm$^2$ was obtained. This value is higher than the threshold density for PCSEL built on SOI under similar conditions. This may be due to the lower optical confinement factor and smaller Q values for the PCSELs built on bulk Si substrate reported here. Notice the calculated Q of 3,000 is much less than Q for PCSEL on SOI. This Q value can be improved to a much higher value, which will result in reduced lasing threshold. A typical spectrum measured above threshold is also shown in Fig. 14(b). The single mode lasing peak wavelength and linewidth are 1,452 nm and 0.87 nm at operation temperature T = 160 K.

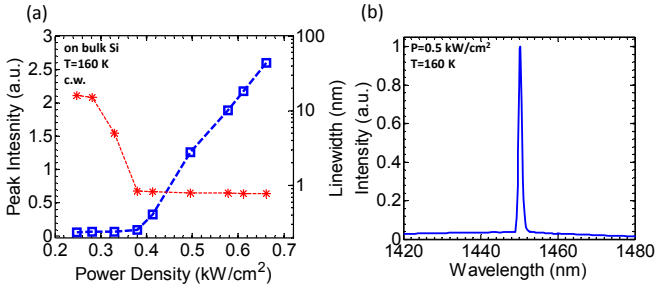


Fig. 14 (a) Lasing intensity and linewidth versus input power density at $T$ = 160 K for PCSEL on bulk Si substrate; (b) Emission spectrum of the laser above threshold.

## IX. PCSEL THERMAL PERFORMANCE ANALYSIS

To evaluate the impact of $SiO_2$ BOX layer on the PCSEL thermal performance, Two PCSELs were built on SOI and on bulk Si substrates, respectively. The laser cavity for both devices is designed to operate at similar temperatures and emission wavelengths. The thicknesses of each layer of the InGaAsP MQW membrane and the parameter of Si-PC are listed in Table 2.

**Table 2** Cavity design structure of laser on bulk Si and SOI.

| Layer materials | Laser on Bulk Si | Laser on SOI |
|---|---|---|
| *p*-InP | 130 nm | |
| InGaAsP MQW | 127 nm | |
| *n*-InP | 130 nm | |
| *n*-InGaAs | 40 nm | |
| Si-PC | 400 nm, $a$ = 540 nm $r/a$ = 0.45 | 190 nm, $a$ = 480 nm $r/a$ = 0.15 |
| SiO2 | 0 | 400 nm |
| Si substrate | 525 μm | |

Thermal resistance is typically used as a figure of merit to quantify the heat dissipation [73, 74]. It can be derived by extracting the shift of emission peak wavelength with varying the temperature and pump power [68]. Spectrum was measured for these two types of lasers under different temperatures and different pump power levels. The results are shown in Fig. 15. The corresponding thermal resistances for PCSELs on bulk Si substrate and on the SOI substrate are calculated to be 303.4 K/W and 558.5 K/W, respectively. This result suggest the impact of SiO2 layer underneath of the PCSELs on SOI substrate present a thermal barrier on the heat dissipation, thur results in higher thermal resistance.

This article has been accepted for publication in a future issue of this journal, but has not been fully edited. Content may change prior to final publication. Citation information: DOI 10.1109/JSTQE.2019.2902904, IEEE Journal of Selected Topics in Quantum Electronics



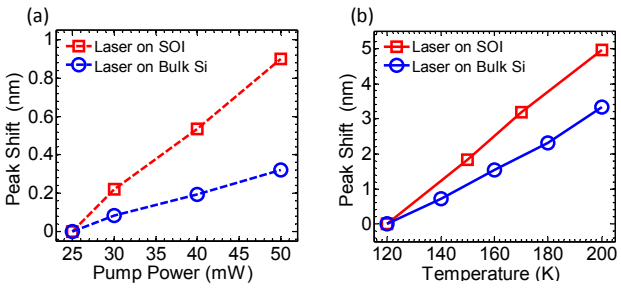


Fig. 15 (a) Emission peak wavelength shift versus pump powers for PC bandedge membrane laser on SOI and on bulk Si substrate. (b) Emission peak wavelength shift versus operation temperatures for PC bandedge membrane laser on SOI and on bulk Si substrate. [68]

## X. Electrically Pumped PCSEL Characterization

Finally, we present some recent results on electrically pumped PCSELs. To realize electrical injection, we introduce here a buried tunnel junction (BTJ) in the InGaAsP MQW heterostructure grown. The BTJ laser serves as the efficient charge injection layer as well as the lateral carrier/optical confinement layer. While BTI structures are widely used in InP based DBR-VCSELs, the major challenge here is the use of BTJs with relatively large aperture sizes, typically ~ 100 μm. Detailed design considerations on the layer thicknesses and doping concentrations should be incorporate in the heterostructure design for proper functions of these BTJ layers.

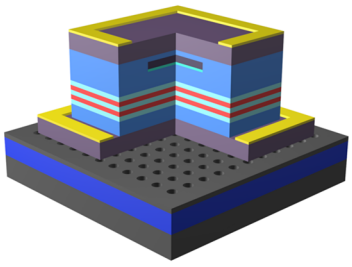

(a)

| Description | Materials | BTJ-PCSEL |
|---|---|---|
| Contact layer: n | InGaAs | 40 nm |
| Cladding layer: n | InP | 80 nm |
| BTJ: $n^{++}$ | InGaAs | 20 nm |
| BTJ: $p^{++}$ | InAlGaAs | 10 nm |
| Cladding layer: p | InP | 265 nm |
| MQW | InGaAsP | 127 nm |
| Cladding layer: n | InP | 31.5 nm |
| Contact layer: n | InGaAs | 40 nm |
| Photonic crystal | air hole Si-PC | 125nm, r/a=0.15 |
| BOX | $SiO_2$ | 400nm |
| Substrate | Si substrate | 525μm |

(b)

Fig. 16. Electrically pumped PCSELs on SOI substrate: (a) Schematic; and (b) Detailed heterostructure and cavity design parameters.

An electrically injected PCSEL on SOI is shown schematically in Fig. 16(a), with detailed layer information shown in Fig. 16(b). A BTJ $n^{++}/p^{++}$ mesa is incorporated in the center of the cavity via two step MOCVD growth process. InGaAsP MQW heterostructure with BTJ and alignment marks were first release from the InP substrate via substrate removal process. The membrane is then transferred onto Si-PC cavity. Careful alignment is carried out to ensure the processed mesa and metal contacts are aligned well with the BTJ mesa, based on the deep etched alignment marks. Standard metallization and mesa etching processes are carried out to form top and bottom ring contacts. PECVD SiO2 layer was deposited as electrical isolation and device planarization layer. Finally, interconnect layer was formed for electrical characterization. The complete device is then mounted on a chip carrier with wire bonding process for device characterization.

The device was characterized at room temperature. Shown in Fig. 17(a) are the measured spectral outputs at different biased currents for an 80 × 80 μm$^2$ BTJ mesa PCSEL device. A dominant single mode lasing emission peak at 1,504 nm appears above the threshold current. Fig. 17(b) shows the light-current-voltage (LIV) characteristics. The turn on voltage is about 0.8 V. The threshold current is about 2 mA.

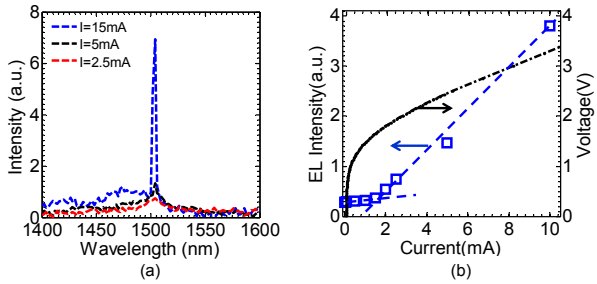


Fig. 17 (a) The emission spectra at different current injection levels measured at room temperature; and (b) The light-current-voltage (LIV) characteristics for an 80x80 μm$^2$ electrically pumped PCSEL on Si.

## XI. Summary

In summary, we review here recent progresses on photonic crystal surface-emitting membrane lasers for on-chip integration with CMOS electronics. Defect free photonic crystal structures are incorporated into laser cavities as ultra-compact membrane reflectors for DBR-free VCSELs and as bandedge cavities evanescently coupled with gain medium for PCSELs. Lateral cavity size effect was also investigated for cavity scaling. Electrically injected PCSELs with BTJ based InGaAsP QW heterostructures were also demonstrated. The use of photonic crystals with different functionalities to construct surface-emitting lasers for on-chip integration opens up a wide range of new device structures for both in-plane and out-of-the-plane (2D and 3D) photonic integration. The membrane transfer printing process developed here also result in heterogeneous integration of dissimilar materials for multi-functional chips with scaling capabilities in integration density and energy efficiency.

Further research is needed to address device efficiencies. While high efficiency VCSELs and PCSELs on native III-V substrates have been reported earlier with wall-plug efficiencies greater than 50%, the efficiencies in the heterogeneously integrated DBR-free MR-VCSELs and Si based PCSELs are largely impacted by the cavity coupling and thin membrane surface and interface qualities. Output power at 10's mW range should be achievable with excellent single mode emission and narrow spectral linewidths. Device scaling in both vertical and lateral directions can also lead to improved device modulation speed and operation data transfer efficiency, with ultimate objective of sub-femto joule per bit energy efficiency.

Thermal and reliability are another set of issues to be addressed. Since photonic bandgap is not essential in these photonic crystal structures reported here, relaxed index contrast is possible to have photonic crystal lasing cavities built on low index contract material systems. However certain index contract is still needed, which may result in the need of low index buffers in the lasing cavity. This issue needs to be further addressed to avoid the use of low index dielectric (e.g. $SiO_2$, $Si_3N_4$, etc.) due to the poor thermal conductivities and the

strain-induced reliabilities issues.

On the other hand, new functional properties should also be expected from photonic crystal surface-emitting membrane lasers, as the modulation of photonic crystal cavity and the gain/loss modulation of the active media can result in lasers with unique spectral, spatial, and beam properties. Engineered beam shapes can be designed. Large area single mode lasers are also feasible. Laser beams can also be steered with certain angles. With the proper dispersion engineering, it is possible to have beam emission in-plane.

## ACKNOWLEDGMENT

The authors acknowledge contributions from collaborators and students involved in the research work reviewed here. We also thank the fabrication support from the University of Texas at Arlington Nanotechnology Research Center, and the University of Texas at Austin, part of NSF NNIN.

## REFERENCES

[1] R. Chen, T. T. D. Tran, K. W. Ng, W. S. Ko, L. C. Chuang, F. G. Sedgwick, and C. Chang-Hasnain, "Nanolasers grown on silicon," *Nat. Photon.,* vol. 5, pp. 170-175, 2011.

[2] D. Liang, G. Roelkens, R. Baets, and J. Bowers, "Hybrid Integrated Platforms for Silicon Photonics," *Materials,* vol. 3, pp. 1782-1802, 2010.

[3] Z. Mi, P. Bhattacharya, J. Yang, and K. Pipe, "Room-temperature self-organised In0. 5Ga0. 5As quantum dot laser on silicon," *Electron. lett.,* vol. 41, pp. 742-744, 2005.

[4] G. Balakrishnan, A. Jallipalli, P. Rotella, S. Huang, A. Khoshakhlagh, A. Amtout, S. Krishna, L. R. Dawson, and D. L. Huffaker, "Room-Temperature Optically Pumped (Al) GaSb Vertical-Cavity Surface-Emitting Laser Monolithically Grown on an Si (1 0 0) Substrate," *IEEE J. Select. Topic. Quant. Electron.,* vol. 12, pp. 1636-1641, 2006.

[5] H. Park, A. W. Fang, O. Cohen, R. Jones, M. J. Paniccia, and J. E. Bowers, "Design and fabrication of optically pumped hybrid silicon-AlGaInAs evanescent lasers," *IEEE J. Select. Topic. Quant. Electron.,* vol. 12, pp. 1657-1663, Nov-Dec 2006.

[6] J. Van Campenhout, P. Rojo Romeo, P. Regreny, C. Seassal, D. Van Thourhout, S. Verstuyft, L. Di Cioccio, J. M. Fedeli, C. Lagahe, and R. Baets, "Electrically pumped InP-based microdisk lasers integrated with a nanophotonic silicon-on-insulator waveguide circuit," *Opt. Express,* vol. 15, pp. 6744-6749, 2007.

[7] S. Stankovic, R. Jones, M. N. Sysak, J. M. Heck, G. Roelkens, and D. Van Thourhout, "1310-nm Hybrid III-V/Si Fabry-Perot Laser Based on Adhesive Bonding," *IEEE Photon. Technol. Lett.,* vol. 23, pp. 1781-1783, Dec 1 2011.

[8] B. B. Bakir, C. Seassal, X. Letartre, P. Viktorovitch, M. Zussy, L. Di Cioccio, and J. M. Fedeli, "Surface-emitting microlaser combining two-dimensional photonic crystal membrane and vertical Bragg mirror," *Appl. Phys. Lett.,* vol. 88, p. 081113, 2006.

[9] G. Roelkens, L. Liu, D. Liang, R. Jones, A. Fang, B. Koch, and J. Bowers, "III-V/silicon photonics for on-chip and intra-chip optical interconnects," *Laser Photon. Rev.,* vol. 4, pp. 751-779, 2010.

[10] O. Painter, R. K. Lee, A. Scherer, A. Yariv, J. D. O'Brien, P. D. Dapkus, and I. Kim, "Two-dimensional photonic band-gap defect mode laser," *Science,* vol. 284, pp. 1819-1821, 06/11/ 1999.

[11] W. Zhou, J. Sabarinathan, P. Bhattacharya, B. Kochman, E. W. Berg, P.-C. Yu, and S. W. Pang, "Characteristics of a photonic bandgap single defect microcavity electroluminescent device," *IEEE J.Quant. Electron.,* vol. 37, pp. 1153-1160, 09// 2001.

[12] H. G. Park, S. H. Kim, S. H. Kwon, Y. G. Ju, J. K. Yang, J. H. Baek, S. B. Kim, and Y. H. Lee, "Electrically Driven Single-Cell Photonic Crystal Laser," *Science,* vol. 305, pp. 1444-7, 2004.

[13] T. Yoshie, A. Scherer, J. Hendrickson, G. Khitrova, H. Gibbs, G. Rupper, C. Ell, O. Shchekin, and D. Deppe, "Vacuum Rabi splitting with a single quantum dot in a photonic crystal nanocavity," *Nature,* vol. 432, pp. 200-203, 2004.

[14] H. Altug, D. Englund, and J. Vučković, "Ultrafast photonic crystal nanocavity laser," *Nat. Phys.,* vol. 2, pp. 484-488, 2006.

[15] S. Noda, "Photonic crystal lasers—ultimate nanolasers and broad-area coherent lasers [Invited]," *J. Opt. Soc. Am. B,* vol. 27, pp. B1-B8, 2010.

[16] K. Hirose, Y. Liang, Y. Kurosaka, A. Watanabe, T. Sugiyama, and S. Noda, "Watt-class high-power, high-beam-quality photonic-crystal lasers," *Nat. Photon.,* vol. 8, pp. 406-411, May 2014.

[17] S. Fan and J. D. Joannopoulos, "Analysis of guided resonances in photonic crystal slabs," *Phys. Rev. B,* vol. 65, p. 235112, 2002.

[18] H. Yang, D. Zhao, S. Chuwongin, J.-H. Seo, W. Yang, Y. Shuai, J. Berggren, M. Hammar, Z. Ma, and W. Zhou, "Transfer-printed stacked nanomembrane lasers on silicon," *Nat. Photon.,* vol. 6, pp. 615-620, 2012.

[19] W. Zhou, D. Zhao, Y.-C. Shuai, H. Yang, S. Chuwongin, A. Chadha, J.-H. Seo, K. X. Wang, V. Liu, and Z. Ma, "Progress in 2D photonic crystal Fano resonance photonics," *Prog. Quant. Electron.,* vol. 38, pp. 1-74, 2014.

[20] H. Yang, D. Zhao, S. Chuwongin, J. H. Seo, W. Yang, Y. Shuai, J. Berggren, M. Hammar, Z. Ma, and W. Zhou, "Transfer-printed stacked nanomembrane lasers on silicon," *Nat. Photon.,* vol. 6, pp. 615-620, 2012.

[21] E. Yablonovitch, "Inhibited spontaneous emission in solid-state physics and electronics," *Phys. Rev. Lett.,* vol. 58, pp. 2059-2062, 1987.

[22] S. Noda, M. Fujita, and T. Asano, "Spontaneous-emission control by photonic crystals and nanocavities," *Nat. Photon.,* vol. 1, pp. 449-458, 2007.

[23] O. Painter, "Two-dimensional photonic band-gap defect mode," *Science,* vol. 284, p. 1999, 1999.

[24] J. Hwang, H. Ryu, D. Song, I. Han, H. Park, D. Jang, and Y. Lee, "Continuous room-temperature operation of optically pumped two-dimensional photonic crystal lasers at 1.6 um," *IEEE Photon. Technol. Lett.,* vol. 12, pp. 1295-1297, 2000.

[25] W. D. Zhou, J. Sabarinathan, P. Bhattacharya, B. Kochman, E. W. Berg, P. C. Yu, and S. W. Pang, "Characteristics of a photonic bandgap single defect microcavity electroluminescent device," *IEEE J.Quant. Electron.,* vol. 37, pp. 1153-1160, 2001.

[26] R. Colombelli, K. Srinivasan, M. Troccoli, O. Painter, C. F. Gmachl, D. M. Tennant, A. M. Sergent, D. L. Sivco, A. Y. Cho, and F. Capasso, "Quantum cascade surface-emitting photonic crystal laser," *Science,* vol. 302, pp. 1374-1377, 2003.

[27] H.-G. Park, S.-H. Kim, S.-H. Kwon, Y.-G. Ju, J.-K. Yang, J.-H. Baek, S.-B. Kim, and Y.-H. Lee, "Electrically driven single-cell photonic crystal laser," *Science,* vol. 305, pp. 1444-1447, 2004.

[28] P. Bhattacharya, J. Sabarinathan, J. Topol'ancik, S. Chakravarty, P. Yu, and W. Zhou, "Quantum dot photonic crystal light sources," *Proc. IEEE,* vol. 93, pp. 1825-1838, 2005.

[29] B. Ellis, M. A. Mayer, G. Shambat, T. Sarmiento, J. Harris, E. E. Haller, and J. Vučković, "Ultralow-threshold electrically pumped quantum-dot photonic-crystal nanocavity laser," *Nat. Photon.,* vol. 5, pp. 297-300, 2011.

[30] S. Wu, S. Buckley, J. R. Schaibley, L. Feng, J. Yan, D. G. Mandrus, F. Hatami, W. Yao, J. Vuckovic, A. Majumdar, and X. Xu, "Monolayer semiconductor nanocavity lasers with ultralow thresholds," *Nature,* vol. doi:10.1038/nature14290, 2015.

[31] M. Imada, S. Noda, A. Chutinan, T. Tokuda, M. Murata, and G. Sasaki, "Coherent two-dimensional lasing action in surface-emitting laser with triangular-lattice photonic crystal structure," *Appl. Phys. Lett.,* vol. 75, p. 316, 1999.

[32] S. Noda, M. Yokoyama, M. Imada, A. Chutinan, and M. Mochizuki, "Polarization Mode Control of Two-Dimensional Photonic Crystal Laser by Unit Cell Structure Design," *Science,* vol. 293, pp. 1123-1125, August 10, 2001 2001.

[33] E. Miyai, K. Sakai, T. Okano, W. Kunishi, D. Ohnishi, and S. Noda, "Photonics: lasers producing tailored beams," *Nature,* vol. 441, pp. 946-946, 2006.

[34] S. L. Chua, L. Lu, J. Bravo-Abad, J. D. Joannopoulos, and M. Soljacic, "Larger-area single-mode photonic crystal surface-emitting lasers enabled by an accidental Dirac point," *Opt. lett.,* vol. 39, pp. 2072-2075, Apr 1 2014.

[35] M. Meier, A. Mekis, A. Dodabalapur, A. A. Timko, R. E. Slusher, J. D. Joannopoulos, and O. Nalamasu, "Laser action from two-

dimensional distributed feedback in photonic crystals," *Appl. Phys. Lett.,* vol. 74, pp. 7-9, 01/04/ 1999.

[36] C. Sciancalepore, B. B. Bakir, X. Letartre, J. Harduin, N. Olivier, C. Seassal, J. Fedeli, and P. Viktorovitch, "CMOS-compatible ultra-compact 1.55- um emitting VCSELs using double photonic crystal mirrors," *IEEE Photon. Technol. Lett.,* vol. 24, pp. 455-457, 2012.

[37] S.-L. Chua, Y. Chong, A. D. Stone, M. Soljacic, and J. Bravo-Abad, "Low-threshold lasing action in photonic crystal slabs enabled by Fano resonances," *Opt. Express,* vol. 19, 1539-62, 2011.

[38] D. S. Song, S. H. Kim, H. G. Park, C. K. Kim, and Y. H. Lee, "Single-fundamental-mode photonic-crystal vertica-cavity surface-emitting lasers," *Appl. Phys. Lett.,* vol. 80, pp. 3901-3, 2002.

[39] N. Yokouchi, A. Danner, and K. D. Choquette, "Two-dimensional photonic crystal confined vertical-cavity surface-emitting lasers," *IEEE J. Sel. Top. Quant. Electron.,* vol. 9, pp. 1439-45, 2003.

[40] R. Magnusson and M. Shokooh-Saremi, "Physical basis for wideband resonant reflectors," *Opt. Express,* vol. 16, pp. 3456-3462, 2008.

[41] V. Karagodsky, F. G. Sedgwick, and C. J. Chang-Hasnain, "Theoretical analysis of subwavelength high contrast grating reflectors," *Opt. Express,* vol. 18, pp. 16973-16988, 2010.

[42] Z. Qiang, H. Yang, S. Chuwongin, D. Zhao, Z. Ma, and W. Zhou, "Design of Fano Broadband Reflectors on SOI," *IEEE Photon. Technol. Lett.,* vol. 22, pp. 1108-1110, 2010.

[43] H. Yang, S. Chuwongin, Z. Qiang, L. Chen, H. Pang, Z. Ma, and W. Zhou, "Resonance control of membrane reflectors with effective index engineering," *Appl. Phys. Lett.,* vol. 95, p. 023110, 2009.

[44] L. Coldren and S. Corzine, *Diode lasers and photonic integrated circuits*: Wiley New York, 1995.

[45] C. Sauvan, J. Hugonin, and P. Lalanne, "Difference between penetration and damping lengths in photonic crystal mirrors," *Appl. Phys. Lett.,* vol. 95, p. 211101, 2009.

[46] D. Zhao, Z. Ma, and W. Zhou, "Field penetrations in photonic crystal Fano reflectors," *Opt. Express,* vol. 18, pp. 14152-14158, 2010.

[47] A. F. Oskooi, D. Roundy, M. Ibanescu, P. Bermel, J. Joannopoulos, and S. G. Johnson, "MEEP: A flexible free-software package for electromagnetic simulations by the FDTD method," *Computer Phys. Communi.,* vol. 181, pp. 687-702, 2010.

[48] D. Zhao, H. Yang, S. Chuwongin, J. H. Seo, Z. Ma, and W. Zhou, "Design of photonic crystal membrane reflector based VCSELs," *IEEE Photon. J.,* vol. 4, pp. 2169-75, 2012.

[49] M. Imada, A. Chutinan, S. Noda, and M. Mochizuki, "Multidirectionally distributed feedback photonic crystal lasers," *Phys. Rev. B,* vol. 65, p. 195306, 2002.

[50] K. Sakai, E. Miyai, T. Sakaguchi, D. Ohnishi, T. Okano, and S. Noda, "Lasing band-edge identification for a surface-emitting photonic crystal laser," *IEEE J. Select. Areas Communi.,* vol. 23, pp. 1335-1340, 07// 2005.

[51] M. Meier, A. Mekis, A. Dodabalapur, A. Timko, R. E. Slusher, J. D. Joannopoulos, and O. Nalamasu, "Laser action from two-dimensional distributed feedback in photonic crystals," *Appl. Phys. Lett.,* vol. 74, pp. 7-9, Jan 4 1999.

[52] D. Zhao, S. Liu, H. Yang, Z. Ma, C. Reuterskiöld-Hedlund, M. Hammar, and W. Zhou, "Printed Large-Area Single-Mode Photonic Crystal Bandedge Surface-Emitting Lasers on Silicon," *Sci. report.,* vol. 6, 2016.

[53] A. C. Masahiro Imada, Susumu Noda, and Masamitsu Mochizuki, "Multidirectionally distributed feedback photonic crystal lasers," *Phys. Rev. B,* vol. 65, p. 195306, 2002.

[54] Y. L. Kazuyoshi Hirose, Yoshitaka Kurosaka, Akiyoshi Watanabe, Takahiro Sugiyama and a. S. Noda, "Watt-class high-power, high-beam-quality photonic-crystal lasers," *Nat. Photon.,* vol. 8, pp. 406-411, 2014.

[55] S. N. Masahiro Imada, Alongkarn Chutinan, Takashi Tokuda, Michio Murata and Goro Sasaki, "Coherent two-dimensional lasing action in surface-emitting laser with triangular-lattice photonic crystal structure," *Appl. Phys. Lett.,* vol. 75, pp. 316-318, 1999.

[56] L. L. Song-Liang Chua, Jorge Bravo-Abad, John D. Joannopoulos, and Marin Soljačić, "Larger-area single-mode photonic crystal surface-emitting lasers enabled by an accidental Dirac point," *Opt. Lett.,* vol. 39, pp. 2072-5, 2014.

[57] A. M. M. Meier, A. Dodabalapur, A. Timko, R. E. Slusher, J. D. Joannopoulos, and O. Nalamasu, "Laser action from two-dimensional distributed feedback in photonic crystals," *Appl. Phys. Lett.,* vol. 74, pp. 7-9, 1999.

[58] M. Y. Susumu Noda, Masahiro Imada, Alongkarn Chutinan, and Masamitsu Mochizuki, "Polarization Mode Control of Two-Dimensional Photonic Crystal Laser by Unit Cell Structure Design," *Science,* vol. 293, pp. 1123-1125, 2011.

[59] B. A. Luis Javier Martınez, Ivan Prieto, J.F. Galisteo-Lopez, Matteo Galli, Lucio Claudio Andreani, Christian Seassal, Pierre Viktorovitch, and Pablo Aitor Postigo, "Two-dimensional surface emitting photonic crystal laser with hybrid triangular-graphite structure," *Opt. Express,* vol. 17, pp. 15043-15051, 2009.

[60] Y. T. Yoshiya Sato, Jeremy Upham, Yasushi Takahashi, Takashi Asano, and Susumu Noda, "Strong coupling between distant photonic nanocavities and its dynamic control," *Nat. Photon.,* vol. 6, pp. 56-61, 2012.

[61] E. M. Kyosuke Sakai, and Susumu Noda, "Coupled-wave model for square-lattice two-dimensional photonic crystal with transverse-electric-like mode," *Appl. Phys. Lett.,* vol. 89, p. 021101, 2006.

[62] Y. Kurosaka, S. Iwahashi, K. Sakai, E. Miyai, W. Kunishi, D. Ohnishi, and S. Noda, "Band structure observation of 2D photonic crystal with various V-shaped air-hole arrangements," *IEICE Electron. Express,* vol. 6, pp. 966-971, 2009.

[63] B. Z. Jeongwon Lee, Song-Liang Chua, Wenjun Qiu, John D. Joannopoulos, Marin Soljacic, and Ofer Shapira, "Observation and differentiation of unique high-Q optical resonances near zero wave vector in macroscopic photonic crystal slabs," *Phys. Rev. Lett.,* vol. 109, p. 067401, Aug 10 2012.

[64] V. Liu and S. Fan, "S4: A free electromagnetic solver for layered periodic structures," *Computer Phys. Communi.,* vol. 183, pp. 2233-2244, 2012.

[65] B. Luk'yanchuk, N. I. Zheludev, S. A. Maier, N. J. Halas, P. Nordlander, H. Giessen, and C. T. Chong, "The Fano resonance in plasmonic nanostructures and metamaterials," *Nat. Mater.,* vol. 9, pp. 707-715, Sep 2010.

[66] Y. Liang, C. Peng, K. Sakai, S. Iwahashi, and S. Noda, "Three-dimensional coupled-wave analysis for square-lattice photonic crystal surface emitting lasers with transverse-electric polarization: finite-size effects," *Opt. Express,* vol. 20, pp. 15945-15961, 2012/07/02 2012.

[67] S.-C. Liu, D. Zhao, X. Ge, C. Reuterskiöld-Hedlund, M. Hammar, S. Fan, Z. Ma, and W. Zhou, "Size Scaling of Photonic Crystal Surface Emitting Lasers on Silicon Substrates," *IEEE Photon. J.,* vol. 10, pp. 1-6, 2018.

[68] S.-C. Liu, D. Zhao, Y. Liu, H. Yang, Y. Sun, Z. Ma, C. Reuterskiöld-Hedlund, M. Hammar, and W. Zhou, "Photonic crystal bandedge membrane lasers on silicon," *Appl. Opt.,* vol. 56, pp. H67-H73, 2017.

[69] K. Hirose, Y. Liang, Y. Kurosaka, A. Watanabe, T. Sugiyama, and S. Noda, "Watt-class high-power, high-beam-quality photonic-crystal lasers," *Nat. Photon.,* vol. 8, p. 406, 04/13/online 2014.

[70] S. Rapp, F. Salomonsson, K. Streubel, S. Mogg, F. Wennekes, J. Bentell, and M. Hammar, "All-epitaxial single-fused 1.55µm vertical cavity laser based on an InP Bragg reflector," *Jpn. J. Appl. Phys,* vol. 38, pp. 1261-1264, 1999.

[71] A. Karim, S. Bjorlin, J. Piprek, and J. Bowers, "Long-wavelength vertical-cavity lasers and amplifiers," *IEEE J.Select. Top. Quant. Electron.,* vol. 6, pp. 1244-1253, 2000.

[72] S. Rapp, J. Piprek, K. Streubel, J. Andre, and J. Wallin, "Temperature Sensitivity of 1.54- m Vertical-Cavity Lasers with an InP-Based Bragg Reflector," *IEEE J. Quant. Electron.,* vol. 33, p. 1839, 1997.

[73] K. H. B. T. Flick, J. Dopke, P. M¨ attig and P. Tepel, "Measurement of the thermal resistance of VCSEL devices," *J. Instrument.,* vol. 6, 2011.

[74] W. Y. James Ferrara, Li Zhu, Pengfei Qiao, and Connie J. Chang-Hasnain1, "Heterogeneously integrated long-wavelength VCSEL using silicon high contrast grating on an SOI substrate," *Opt. Express,* vol. 23, pp. 2512-2523, Feb 09 2015.

**Weidong Zhou** (M'01, SM'08) obtained his BS and ME degrees from Tsinghua University, Beijing, China, in 1993 and 1996, respectively, and his PhD degree from University of Michigan, Ann Arbor in 2001. He is currently a Distinguished University Professor at the University of Texas at Arlington (UTA). Before joining UTA, he worked as a lead engineer at CIENA corporation for three years. Dr. Zhou and his group have been working in the area of photonic crystal membrane photonics, especially membrane lasers, imagers, and sensors, for integrated silicon photonics and flexible optoelectronics. Dr. Zhou has authored and co-authored over 330 journal publications and conference presentations, including over 60 invited conference talks.

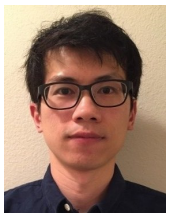

**Shih-Chia Liu** received his BS degree in Physics from Chung Cheng University, Taiwan, and MS degree in Electro-Optical Engineering from Chiao Tung University, Taiwan, in 2008, and his PhD degree in Electrically Engineering from University of Texas at Arlington, USA, in 2017. From 2008 to 2012, he was a R&D Engineer with Innolux Corporation, Taiwan. From 2012 to 2017, he was a Research Assistant with Dr. Weidong Zhou`s Nanophotonics Laboratory. His doctoral research involved the design, fabrication, and characterization of photonic crystal surface emitting laser on silicon substrate. He is currently a R&D Engineer with Applied Optoelectronics, Sugar Land, Texas. His current research focuses on silicon and integrated photonics for datacom and telecom.

**Xiaochen Ge** (M'17) received the B.S. degree in electronic science and technology from Sichuan University, Chengdu, China in 2009 and the Ph.D. degree in optical engineering from Zhejiang University, Hangzhou, China in 2015. Since 2015 he has been a Faculty Associate Researcher in University of Texas at Arlington, Arlington, TX, USA. His research interest includes photonic crystals and integrated photonics. Currently he is working on 2D material based photonic devices.

**Deyin Zhao** received the M.S. degree in Physics from Shanghai University in 2005 and the Ph.D. degree in Optoelectronics from Shanghai Institute of Micro-systems and information technology, China in 2008. From 2008 to 2017, he was a researcher in the Nanophotonics Lab at University of Texas, Arlington and also worked as an optical scientist in Semerane Inc. He has authored and co-authored around 40 articles in international journals. His research interests are in the areas of vertical cavity surface emitting lasers (VCSEL), edge emitting lasers, modulators and waveguide couplers. Currently he is working at MACOM on the development of high speed lasers and photodetectors.

**Hongjun Yang** received his BS and MS degrees from Jilin University, Changchun, China, and his PhD degree from University of Texas at Arlington (UTA), all in electrical engineering. He is currently a statistician at Abbott Laboratories, Irving, TX. Before that, he worked as a faculty research associate at UTA for two years. Dr. Yang has authored and co-authored over 50 journal publications and conference presentations.

**Carl Reuterskiöld Hedlund** obtained his M.Sc. in materials physics at the Royal Institute of Technology in Stockholm, Sweden. He joined the Department of Electronics in 2013 where he is currently pursuing a Ph.D. His main field of research includes crystal growth by MOVPE as well as design and fabrication of semiconductor lasers, including Photonic Crystal-VCSELs, Transistor-VCSELs, and other electronic and optoelectronic devices.

**Mattias Hammar,** received his MSc (1986) and PhD (1993) degrees from the Department of Physics, Royal Institute of Technology (KTH). From 2007 he is a Professor at the Department of Electronics at KTH and during his career he has also been affiliated with the Swedish Institute of Microelectronics, IBM Research Division and Zarlink Semiconductor. He has an extensive academic and industrial experience related to optoelectronic materials and devices, he has managed or been involved in several national and international projects within the photonics area, and he is Program Director for the International Master's program in Nanotechnology at KTH.